THE JOURNAL OF PHYSICAL CHEMISTRY C
A JOURNAL OF THE AMERICAN CHEMICAL SOCIETY

pubs.acs.org/JPCC

Article

Lattice Effect on the Superexchange Interaction in Antiferromagnetic $Bi_{2.1}Sr_{1.9}CaCu_2O_{8+\delta}$

Jie Xin, Alexander G. Gavriliuk, Jia-Wei Hu, Jian-Bo Zhang, Gen-Da Gu, Alexander F. Goncharov, Hai-Qing Lin, Ho-Kwang Mao, Xiao-Jia Chen, and Viktor V. Struzhkin*

Cite This: J. Phys. Chem. C 2024, 128, 7223−7234

Read Online

ABSTRACT: By employing Raman scattering and X-ray diffraction techniques on antiferromagnetic $Bi_{2.1}Sr_{1.9}CaCu_2O_{8+\delta}$ within the same pressure conditions, we tracked the evolution of the two-magnon spectrum and structural parameters under pressures of up to nearly 30 GPa. Consequently, we established the relationship between pressure, in-plane lattice parameter *d*, and superexchange interaction *J* as $J \sim d^{-(6.6\pm0.2)}$. Within the examined pressure range, this compound did not exhibit superconductivity, as determined by a sensitive magnetic measurement technique. Additionally, we observed phonon anomalies, suggesting possible disorder effects in Bi−O layers and reduced charge transfer from these layers, particularly above 10 GPa. We discuss the impacts of pressure and chemical doping on *J* and the structure, along with their implications for superconductivity.

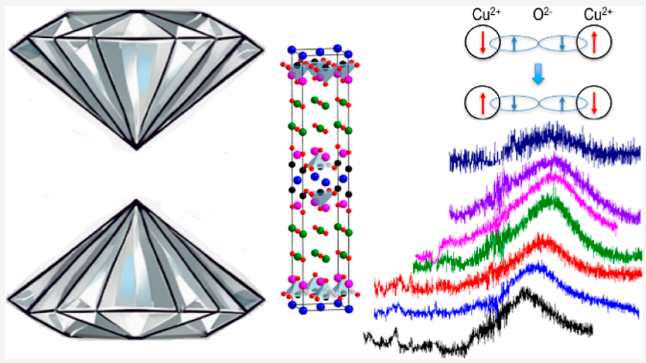

1. INTRODUCTION

Since the discovery of high-temperature superconductivity in cuprates,[1,2] extensive experimental and theoretical research has yielded many important findings. However, achieving a comprehensive theoretical understanding of superconductivity in cuprates is still challenging. The resonating valence bond[3,4] and spin-fluctuation-mediated scenarios[5,6] stand out as the most promising theoretical approaches to describe superconductivity in cuprates. In these spin-related theories, the Cu−O−Cu superexchange interaction, denoted by *J*, is considered to be the cause of electron pairing. In the spin-fluctuation-mediated scenario, electron pairing occurs through the exchange of magnetic spin fluctuations, also governed by *J*.[6] The value of *J* can be conveniently determined from the two-magnon spectrum using Raman scattering spectroscopy.[7] Following the discovery of superconductivity in these two families, the quantitative determination of *J* for antiferromagnetic La_2CuO_4[8−10] and $YBa_2Cu_3O_6$[11] has been achieved using Raman scattering spectroscopy. Extensive experiments have further revealed that *J* changes with doping in a manner similar to the pseudogap and pair peak across almost all cuprate superconductors.[9,11−15] These similarities suggest that high-energy magnetic fluctuations are likely involved in the formation of both the pseudogap and the Cooper pairing. Coherent charge fluctuation spectroscopy[16] suggests this evolution from high-energy excitations to superconducting quasiparticles. Theoretical models have successfully reproduced the transition from the two-magnon peak to a quasiparticle response as doping increases.[17] Interestingly, reports indicate an approximate linear relationship between *J* and the maximum critical temperature, T_c, in many optimally doped cuprates.[18] These findings underscore the significance of *J* and its connection to superconductivity in cuprates. Emphasizing the importance of this parameter in understanding superconductivity necessitates a quantitative relationship between the lattice parameter and *J*. However, obtaining such information from existing experiments across various superconducting families is rare and challenging.[8−15,18,19]

Applying pressure has been proven to provide a clean and effective tool to tune the structural, magnetic, and superconducting properties.[20] At high pressures, Raman spectra can be collected for various materials, including cuprates.[21] Using Raman spectroscopy, the two-magnon spectra under high pressure of parent compounds from two key cuprate families have been obtained.[22−25] High-pressure behaviors of *J* have been established for La_2CuO_4,[22] Eu_2CuO_4,[23,25] $Sr_2CuCl_2O_2$,[24] and $YBa_2Cu_3O_{6.2}$.[25] The complex theoretical expression for *J* is

Received: December 18, 2023
Revised: April 8, 2024
Accepted: April 11, 2024
Published: April 22, 2024

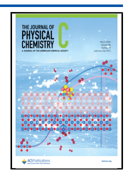

https://doi.org/10.1021/acs.jpcc.3c08244
J. Phys. Chem. C 2024, 128, 7223−7234

traditionally simplified to a power law, $J \sim d^{-n}$, where d represents the in-plane Cu−O−Cu bond length and n is an empirically determined constant. Establishing the precise relationship between d and J requires determining the material's structural evolution under consistent conditions of composition, temperature, and pressure. The literature provides estimated relationships, such as $J \sim d^{-(6.4\pm0.8)}$[22] for La_2CuO_4 and $J \sim d^{-(3.0\pm0.5)}$[25] for Eu_2CuO_4 and $YBa_2Cu_3O_{6.2}$, respectively, based on structural information. The empirical constant, n, closely aligns with the value found in $J \sim d^{-(4\pm2)}$ for M_2CuO_4 (M = Pr, Nd, Sm, Eu, and Gd).[19] Experiments using neon as a pressure medium on the insulating compound, $Bi_{1.98}Sr_{2.06}Y_{0.68}CaCu_2O_{8+\delta}$, resulted in $J \sim d^{-(10.33)}$.[26] It is unclear if the large n value stems from lattice distortion or internal pressure due to Y substituting for Ca in the system.[27] To date, an accurate relationship for an antiferromagnetic parent cuprate, based on simultaneous spectroscopy and diffraction measurements under the same pressure conditions, has not yet been established. This is obviously an urgent subject in order to elucidate the spin-related pairing mechanism for superconductivity in high-T_c cuprates.

This work is designed to solve the problem mentioned above with the help of high-quality single crystals of $Bi_2Sr_2CaCu_2O_{8+\delta}$ (Bi-2212). The composition choice of the samples hopes to eliminate the possible external effect resulting from the elemental substitution and draw the information solely due to the application of pressure. After characterizing the antiferromagnetic feature of the chosen single crystal $Bi_{2.1}Sr_{1.9}CaCu_2O_{8+\delta}$, we performed high-pressure Raman scattering and X-ray diffraction (XRD) to obtain the spectroscopic and structural properties at high pressures. The evolution of the two-magnon spectrum with pressure for $Bi_{2.1}Sr_{1.9}CaCu_2O_{8+\delta}$ is obtained after the comparison of the spectroscopic character of nearly optimally doped $Bi_{2.1}Sr_{1.9}CaCu_2O_{8+\delta}$ loaded together in the sample chamber near antiferromagnetic $Bi_{2.1}Sr_{1.9}CaCu_2O_{8+\delta}$. The pressure (or lattice parameter) dependence of J is determined for antiferromagnetic $Bi_{2.1}Sr_{1.9}CaCu_2O_{8+\delta}$. Within the studied pressure regime and the same pressure environment, the idea of pressure-induced superconductivity in antiferromagnetic $Bi_{2.1}Sr_{1.9}CaCu_2O_{8+\delta}$ is experimentally examined based on a highly sensitive magnetic detection technique. We also discuss the possible factors controlling superconductivity from the comparisons of the present and available experiments.

This study aims to address the identified issue using high-quality $Bi_2Sr_2CaCu_2O_{8+\delta}$ (Bi-2212) single crystals. We selected the sample composition to negate potential external effects from elemental substitution, focusing exclusively on pressure-induced changes. Following the characterization of the antiferromagnetic properties of $Bi_{2.1}Sr_{1.9}CaCu_2O_{8+\delta}$, we conducted high-pressure Raman scattering and XRD measurements to explore its spectroscopic and structural properties under pressure. We determined the evolution of the two-magnon spectrum under pressure for $Bi_{2.1}Sr_{1.9}CaCu_2O_{8+\delta}$ by comparing it with the spectroscopic characteristics of a nearly optimally doped sample placed in proximity to the same chamber. We established the pressure (or lattice parameter) dependence of J for antiferromagnetic $Bi_{2.1}Sr_{1.9}CaCu_2O_{8+\delta}$. We experimentally investigated pressure-induced superconductivity in antiferromagnetic $Bi_{2.1}Sr_{1.9}CaCu_2O_{8+\delta}$ within the designated pressure regime by using a highly sensitive magnetic detection technique. We also discuss the possible factors controlling superconductivity from the comparisons of the present and available experiments.

2. EXPERIMENTAL DETAILS

The single crystals of Bi-2212 grown using a floating zone technique were detailed previously.[28] Because of the Bi−Sr mixing in the Sr_2O_2 layers, the as-grown crystal composition is $Bi_{2.1}Sr_{1.9}CaCu_2O_{8+\delta}$. The extra oxygen atoms were removed by annealing under vacuum carried out in sealed quartz tubes. In order to achieve the lowest possible oxygen doping level, nonsuperconducting $Bi_{2.1}Sr_{1.9}CaCu_2O_{8+\delta}$ crystal with T_c = 0 K used in this work was annealed under vacuum of 10^{-3} Torr at 500 °C for 30 days. However, we do not know what the exact oxygen content is in the crystal.

Magnetization measurements were used to characterize the magnetic feature and superconducting transition of the synthesized samples by combining a superconducting quantum interference device magnetometer (Quantum Design MPMS3) and an in-house highly sensitive magnetic detection instrument. The latter was developed for detecting superconductivity for the sample with small dimensions in a diamond anvil cell (DAC) at high pressures.[20,29,30] This technique is based on suppression of the Meissner effect and quenching of superconductivity in the sample by an external magnetic field. The magnetic field applied to the sample inserted into the DAC mainly affects the signal coming from the sample. If the sample is superconducting, its transition temperature can be identified at the point where the signal goes to zero due to the disappearance of the Meissner effect. This highly sensitive technique has been used to discover superconductivity in compressed sulfur[31] and lithium[32] and study the pressure effect on T_c in conventional superconductor NbN[33] and various cuprates including $YBa_2Cu_3O_{7-\delta}$,[34] $Bi_2Sr_2Ca_{n-1}Cu_nO_{2n+4+\delta}$ (n = 2,3),[30,35] $Tl_2Ba_2CaCu_2O_{8+\delta}$,[36] and $HgBa_2CuO_{4+\delta}$.[37]

In the current study, we loaded nearly optimally doped $Bi_{2.1}Sr_{1.9}CaCu_2O_{8+\delta}$ crystal as a reference and an antiferromagnetic $Bi_{2.1}Sr_{1.9}CaCu_2O_{8+\delta}$ crystal separately into a DAC. The crystal was cut in the dimensions of approximately 100 × 100 × 20 μm^3. It was loaded with a ruby chip together into a sample chamber in a gasket made by nonmagnetic Ni−Cr alloy. The gasket is pressed in between two diamond anvils with a diameter of 300 μm in a DAC made by nonmagnetic Be−Cu alloy. The layout of such instruments and designs was given in detail previously.[20,29,30] The DAC was then mounted in a low-temperature cryostat with accessible optical windows, manufactured from Cryo Industries of America, lnc. The pressure can be mechanically tuned at the required pressure and temperature. In such a design, the Raman spectrum of the sample in DAC can be collected at the desired temperature and pressure. The temperature was monitored from the silicon diode sensor attached to the DAC in close proximity to the sample with a typical precision of ±0.5 K. The pressure level was gauged based on the shift of the R1 fluorescence line of ruby[38] with the correction of the temperature effect. For high-pressure magnetic susceptibility measurements, we changed and measured the pressure at a temperature of about 120 K. Below this temperature, the pressure can maintain a nearly constant value at low temperatures for the DAC and gasket in such an instrument.

To have consistency of the spectroscopy and structure data for the comparison, we conducted measurements of high-pressure Raman scattering (including both two-magnon and phonon Raman experiments) and XRD measurements on

https://doi.org/10.1021/acs.jpcc.3c08244
J. Phys. Chem. C 2024, 128, 7223−7234

$Bi_{2.1}Sr_{1.9}CaCu_2O_{8+\delta}$ at room temperature. In fact, the spectroscopic signature of the two-magnon scattering for our studied $Bi_{2.1}Sr_{1.9}CaCu_2O_{8+\delta}$ is not strong. For comparison, we loaded this crystal together with a nearly optimally doped crystal nearby into a sample chamber (about 120 μm in diameter and 30 μm in thickness) of a DAC with a pair of diamond anvils with a diameter of 300 μm. Both crystals were freshly cleaved with shining surfaces. A chip of ruby was put near the edge of the chamber filled with neon as the pressure medium. The Raman scattering signal was created by the Coherent sapphire laser device with 488 nm wavelength to illuminate an approximate 5 × 5 μm^2 spot on the crystal surface. The collected Raman signals are all illuminated at the same position on each sample at different pressures. The low 2 mW power of the laser was chosen in order to avoid the overheating of the sample. Raman spectra were collected in the backscattering geometry using a low-resolution (broad spectral range) 300 g/mm grating. For each pressure of interest, we collected the Raman spectra of the two crystals one by one by keeping the same measurement conditions, such as collecting time and laser grating. The Raman spectrum of the nearly optimally doped $Bi_{2.1}Sr_{1.9}CaCu_2O_{8+\delta}$ at each studied pressure exhibits a nearly flat background in the two-magnon scattering wavenumber range. The weak two-magnon scattering spectrum of antiferromagnetic $Bi_{2.1}Sr_{1.9}CaCu_2O_{8+\delta}$ at the same pressure can be picked up and enlarged by subtracting the nearly flat background from nearly optimally doped $Bi_{2.1}Sr_{1.9}CaCu_2O_{8+\delta}$. In a separate high-pressure experiment, we measured evolution of the phonon part of the Raman spectra of the antiferromagnetic $Bi_{2.1}Sr_{1.9}CaCu_2O_{8+\delta}$ sample to 31.5 GPa using a high-resolution 1200 g/mm grating.

Synchrotron XRD experiments were conducted at the 16BM-D beamline of the High Pressure Collaborative Access Team (HPCAT) at the Advanced Photon Source (APS) of Argonne National Laboratory, with an incident X-ray wavelength of 0.424603 Å. The antiferromagnetic $Bi_{2.1}Sr_{1.9}CaCu_2O_{8+\delta}$ crystal was finely ground into powders to obtain good diffraction data. The powders were pressed into a small piece. It was then loaded into a symmetric DAC with anvils in a diameter of 300 μm together with a small ruby chip to monitor the pressure. Neon was used as the pressure-transmitting medium. The diffraction patterns were collected at room temperature at pressures of up to 34 GPa. The two-dimensional patterns were integrated into 2θ vs intensity data using Fit2D software.[39] The diffraction patterns were analyzed using the Le Bail method in terms of the GSAS-II package.[40]

It should be mentioned that in all these measurements, the samples were kept in the neon environment. The experimental data for antiferromagnetic $Bi_{2.1}Sr_{1.9}CaCu_2O_{8+\delta}$ were collected and analyzed on the same single crystal. These considerations are expected to provide consistent and reliable data of the studied system.

3. RESULTS AND DISCUSSION

3.1. Sample Characterization. The characterization of the quantum ground state of antiferromagnetic $Bi_{2.1}Sr_{1.9}CaCu_2O_{8+\delta}$ is given from the magnetization measurements (Figure 1). There is an antiferromagnetic−paramagnetic transition at the Néel temperature (T_N) of 90 K, indicated by the kink in the temperature dependence of the magnetic moment in a magnetic field directed along the c axis. No evidence for supporting superconductivity is provided from the magnetic susceptibility data down to 2 K. The kink for the antiferromagnetic transition in studied antiferromagnetic $Bi_{2.1}Sr_{1.9}CaCu_2O_{8+\delta}$ is similar to those found in other antiferromagnetic cuprates such as $Bi_2Sr_2Ca_{1-x}Y_xCu_2O_{8+\delta}$,[41] $La_2CuO_{4+\delta}$,[42] and $Bi_2SrLaCuO_y$.[43] No magnetic phase transition has ever been reported for Bi-2212.[43] The T_N value obtained for the studied antiferromagnetic $Bi_{2.1}Sr_{1.9}CaCu_2O_{8+\delta}$ compound is 20 K higher than those in the $Bi_2Sr_2Ca_{1-x}Y_xCu_2O_{8+\delta}$ system.[41] This result confirms the strong antiferromagnetic properties of our sample. The relatively high T_N also correlates with minimal excess oxygen content. Consequently, we possess a $Bi_{2.1}Sr_{1.9}CaCu_2O_{8+\delta}$ sample with typical composition and antiferromagnetic properties for future research.

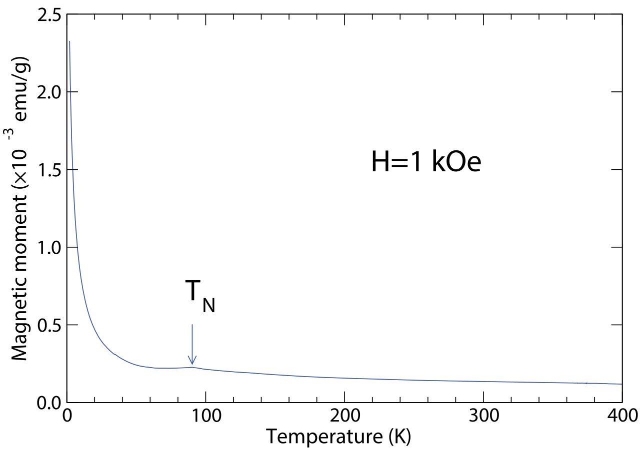

Figure 1. Temperature dependence of the magnetic susceptibility of antiferromagnetic $Bi_{2.1}Sr_{1.9}CaCu_2O_{8+\delta}$ measured with a magnetic field of 1 kOe at ambient pressure.

3.2. Two-Magnon Scattering at High Pressures. Antiferromagnetism stands out as a key physical characteristic of parent cuprates. Classical spin waves resemble acoustics, rendering magnon (single-spin flip) excitations nearly undetectable in inelastic light scattering. However, two adjacent spins on the Cu sites, linked by oxygen ions, can simultaneously reverse their directions. This process adheres to the selection rules for the two-magnon process allowed for Raman scattering. Raman scattering can directly probe the double spin-flop excitations (two-magnon) in CuO_2 layers. Since reversing two adjacent spins simultaneously consumes energy equivalent to six nearest superexchange coupling constants, the two-magnon peak is expected to manifest at around 3J in energy. Owing to magnon−magnon interactions, the ratio deviates slightly from 3, settling at 2.7 as per the two-dimensional Heisenberg model.[44]

For a parent cuprate, previous Raman scattering studies detected the two-magnon peak around 3000 cm^{-1} at ambient pressure, corresponding to a J of ~1000 cm^{-1} (about 125 meV).[8−11] This spectrum range overlaps with the two-phonon Raman peak of the diamond (around 2500 cm^{-1}). Therefore, the collection of the two-magnon spectrum is a challenge by using diamond anvils. This is probably a reason why the high-pressure behaviors of the two-magnon Raman scattering for many parent cuprates have not been reached yet. To solve this critical problem, we loaded the antiferromagnetic $Bi_{2.1}Sr_{1.9}CaCu_2O_{8+\delta}$ crystal together with nearly optimally doped $Bi_{2.1}Sr_{1.9}CaCu_2O_{8+\delta}$ into a DAC (inset of Figure 2a). By performing the measurements at the same conditions, we obtained their Raman spectra. As an example, Raman spectra

https://doi.org/10.1021/acs.jpcc.3c08244
J. Phys. Chem. C 2024, 128, 7223−7234

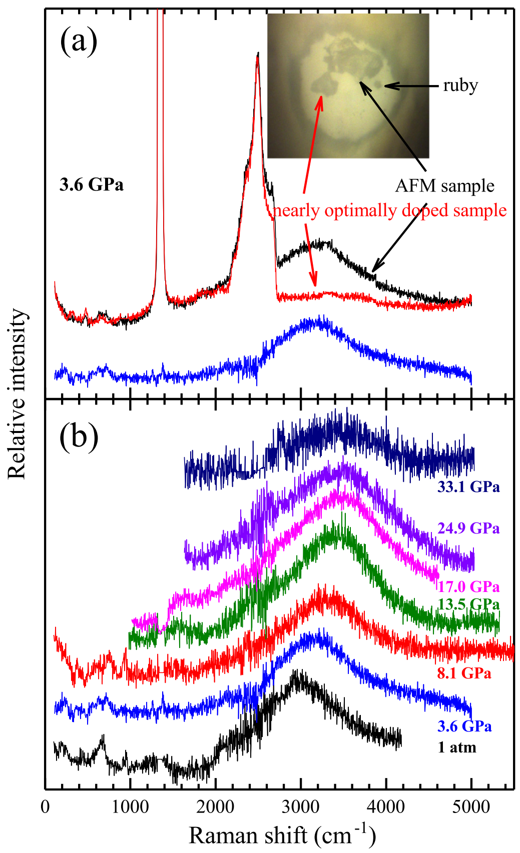

Figure 2. Two-magnon Raman scattering spectra for antiferromagnetic $Bi_{2.1}Sr_{1.9}CaCu_2O_{8+\delta}$ under pressure. (a) Raman spectra of the antiferromagnetic (black curve) and nearly optimally doped (red curve) $Bi_{2.1}Sr_{1.9}CaCu_2O_{8+\delta}$ at a pressure of 3.6 GPa. The blue curve corresponds to the spectrum subtraction from the signal of the antiferromagnetic sample to that of the nearly optimally doped one. Inset: photograph of two crystals in a neon environment with a ruby chip. (b) Subtracted two-magnon scattering spectra of antiferromagnetic $Bi_{2.1}Sr_{1.9}CaCu_2O_{8+\delta}$ at representative pressures in the compression run.

at 3.6 GPa are shown in Figure 2a. With the assumption of the same active Raman feature from the used diamond anvils or medium for the two studied crystals at the measured pressure, the strong two-magnon scattering spectrum can be derived by subtracting the collected spectrum from that of nearly optimally doped $Bi_{2.1}Sr_{1.9}CaCu_2O_{8+\delta}$. This procedure turned out to be very successful. As can be seen, the two-magnon frequency of antiferromagnetic $Bi_{2.1}Sr_{1.9}CaCu_2O_{8+\delta}$ at ambient pressure is well situated in the trend of Bi-2212 with the different dopants.[12,13] The positions of the phonon modes at the low wavenumbers are also consistent with those reported from Raman measurements.[45,46]

Previous Raman scattering research on parent cuprates identified the two-magnon peak near 3000 cm^{-1} under ambient pressure, equating to a J value of approximately 1000 cm^{-1} (around 125 meV). This spectral range coincides with the two-phonon Raman peak of diamond, which is around 2500 cm^{-1}. Consequently, collecting the two-magnon spectrum using diamond anvils presents a significant challenge. This likely explains why the high-pressure behaviors of two-magnon Raman scattering in many parent cuprates remain unexplored. To address this issue, we placed both an antiferromagnetic $Bi_{2.1}Sr_{1.9}CaCu_2O_{8+\delta}$ crystal and a nearly optimally doped $Bi_{2.1}Sr_{1.9}CaCu_2O_{8+\delta}$ crystal into a DAC, as shown in the inset of Figure 2a. Conducting measurements under identical conditions, we acquired their Raman spectra. For instance, Figure 2a displays the Raman spectrum at 3.6 GPa. Assuming identical Raman features from the diamond anvils or pressure medium for both crystals at the tested pressure, the distinct two-magnon scattering spectrum was isolated by subtracting the nearly optimally doped $Bi_{2.1}Sr_{1.9}CaCu_2O_{8+\delta}$ spectrum from the collected one. This method proved to be highly successful. Additionally, the phonon mode positions at low wavenumbers match those reported in previous Raman studies. Figure 2b presents the two-magnon Raman scattering spectra for antiferromagnetic $Bi_{2.1}Sr_{1.9}CaCu_2O_{8+\delta}$ under pressures of up to 33.1 GPa. The two-magnon scattering signal was captured throughout both compression and decompression runs. With increasing pressure, the two-magnon peak broadens, shifts to higher wavenumbers (or energies), and diminishes in intensity. Such behaviors align with earlier findings for La_2CuO_4 up to 10 GPa,[22] Eu_2CuO_4 up to 41 GPa,[25] $YBa_2Cu_3O_{6.2}$ up to 43 GPa,[25] and $Bi_{1.98}Sr_{2.06}Y_{0.68}CaCu_2O_{8+\delta}$ up to 32 GPa.[26]

Figure 3 depicts the evolution of the two-magnon frequency (ω_{2M}) with the pressure for antiferromagnetic

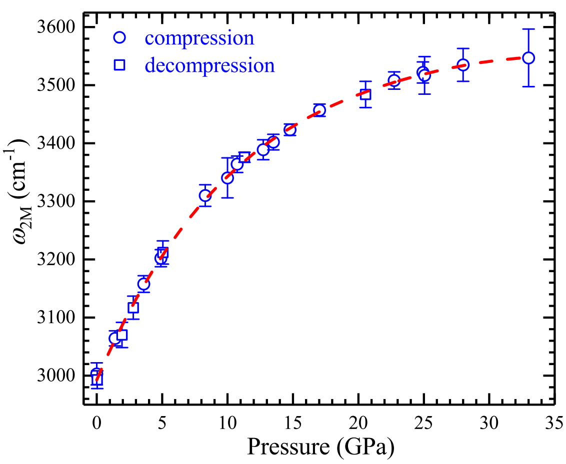

Figure 3. Pressure dependence of the two-magnon frequency in antiferromagnetic $Bi_{2.1}Sr_{1.9}CaCu_2O_{8+\delta}$ in the compression and decompression run. The dashed curve is the polynomial fitting to the data points for the guide to the eyes.

$Bi_{2.1}Sr_{1.9}CaCu_2O_{8+\delta}$. ω_{2M} continuously rises from approximately 3000−3550 cm^{-1} with increasing pressure, a trend also observed in La_2CuO_4,[22] $Sr_2CuCl_2O_2$,[24] and $Bi_{1.98}Sr_{2.06}Y_{0.68}CaCu_2O_{8+\delta}$.[26] It is noteworthy that early studies observed a nearly linear change of ω_{2M} with pressure in Eu_2CuO_4[25] and $YBa_2Cu_3O_{6.2}$.[25] The increase of ω_{2M} in antiferromagnetic $Bi_{2.1}Sr_{1.9}CaCu_2O_{8+\delta}$ up to 33 GPa closely mirrors that of La_2CuO_4[22] within 10 GPa. In contrast, $Bi_{1.98}Sr_{2.06}Y_{0.68}CaCu_2O_{8+\delta}$[26] shows a significant increase of ω_{2M} from a similar starting point to over 4000 cm^{-1}, within a comparable pressure range to this study. Across all of these cuprate measurements, an increase in ω_{2M} with lattice compression is a common occurrence. This trend can be seen as a characteristic feature of ω_{2M} for cuprates under a high pressure.

Superconductivity in cuprates develops through the suppression of the antiferromagnetic order with doping. Earlier publications have generally suggested that applying pressure

https://doi.org/10.1021/acs.jpcc.3c08244
J. Phys. Chem. C 2024, 128, 7223−7234

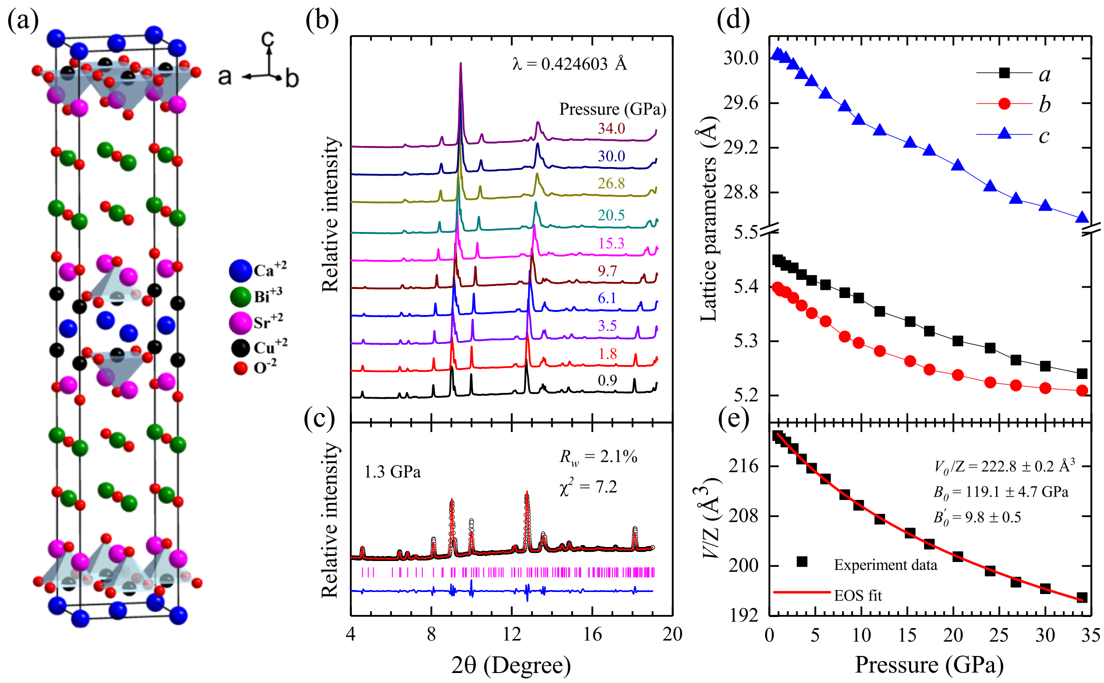

Figure 4. Structural properties of antiferromagnetic $Bi_{2.1}Sr_{1.9}CaCu_2O_{8+\delta}$ at high pressures. (a) Schematic orthorhombic structure with the space group of *Amaa*. (b) Integrated XRD data at representative pressures. (c) Observed XRD patterns (circles), Le Bail fitting (red line), and their difference (blue line) between the observed and calculated profiles at a pressure of 1.3 GPa. The vertical bars refer to the peak positions. (d) Lattice parameters along the *a*, *b*, and *c* axes as a function of pressure. (e) Pressure dependence of the unit-cell volume V/Z.

affects superconductivity similarly to chemical doping in these compounds (see ref 35 and references therein). Recent findings, however, indicate a pressure-induced transition to an insulating state in Bi-2212 superconductors,[47] casting doubt on the continuous pressure-driven charge (holes) transfer into Cu−O planes in cuprates. Hall effect studies up to 18 GPa support this charge-transfer model, showing a reduction in Hall coefficient R_H. However, R_H remains nearly constant and even slightly increases above 18 GPa. The nonmonotonic behavior of R_H has been interpreted as resulting from a quantum phase transition of unknown origin.[47] Notably, the behavior of the two-magnon peak with doping contrasts with its response to pressure. Upon doping, the two-magnon Raman peak broadens and shifts to a lower wavenumber.[9,11−15,48,49]

Recent resonant X-ray scattering (RIXS) experiments suggest that J remains constant with doping, in contrast to earlier Raman scattering studies that demonstrate a suppression of the two-magnon peak energy due to doping. RIXS measurements indicate that J is an intrinsic property of the compound system, showing minimal sensitivity to doping levels (see Discussion and ref 18). The theoretical study[17] shows that even when J (specifically, parameters t and U) is held constant, the two-magnon peak energy still varies with doping. Therefore, this approach suggests that the two-magnon peak reflects an effective J (J_{eff}), reduced by the presence of charge carriers in the CuO_2 planes. The two-magnon "edge" shows minimal dependence on doping,[15] yet the peak position of the two-magnon response—a common indicator of superexchange interaction—exhibits noticeable softening with doping. Although RIXS results hint at single-magnon-like excitations being less affected by doping, a comprehensive analysis of RIXS's doping dependence in cuprate systems has yet to be conducted. The potential discrepancy between the doping effects on single-magnon-like excitations in RIXS and two-magnon excitations in Raman analysis warrants further experimental and theoretical investigation. The maximum T_c in a family of cuprates may be indeed proportional to bare J, as RIXS results suggest,[18] but T_c at a specific doping level likely depends on J_{eff}, influenced by charge fluctuations in the material. Using bare J as the metric for T_c fails to account for the reduced T_c in heavily overdoped materials. For clarity in future discussions, we will use the notation J to denote the superexchange parameter derived from the two-magnon Raman peak.

3.3. Structural Evolution with Pressure. To explore how the two-magnon peak energy ω_{2M} (thus J) changes with lattice parameters, we performed synchrotron XRD measurements on the antiferromagnetic compound $Bi_{2.1}Sr_{1.9}CaCu_2O_{8+\delta}$ under pressures up to 34 GPa. Figure 4a depicts the schematic crystal structure of this material, which belongs to the *Amaa*[50] space group. This structure features two equivalent perovskite subcells aligned diagonally in the a−b plane and bonded by van der Waals forces. Each subcell comprises two insulating BiO layers and two SrO layers. Within each subcell, a Ca layer separates two structurally identical CuO_2 layers. The layers are stacked in a BiO−SrO−CuO_2−Ca−CuO_2−SrO−BiO sequence.

Figure 4b presents the powder XRD results for antiferromagnetic $Bi_{2.1}Sr_{1.9}CaCu_2O_{8+\delta}$ under high pressures at room temperature. Upon application of pressure, all diffraction peaks shift to higher angles, indicating lattice contraction. No new diffraction peaks emerged. Additionally, no peak merging or splitting was observed. These findings suggest the absence of structural transformations under pressure. The compound retains its structure within the studied pressure range, aligning with earlier high-pressure structural investigations of this system.[51,52]

https://doi.org/10.1021/acs.jpcc.3c08244
J. Phys. Chem. C 2024, 128, 7223−7234

Refining the crystal structure of Bi-2212 presents significant challenges. We contend that Le Bail fitting to the average structure model can accurately determine the lattice parameters. Figure 4c shows the powder XRD data and Le Bail fitting for antiferromagnetic $Bi_{2.1}Sr_{1.9}CaCu_2O_{8+\delta}$ at a pressure of 1.3 GPa, based on the structure model in Figure 4a. The fitting yields reasonable factors, with $R_\omega = 2.1\%$ and $\chi^2 = 7.2$. Similar fittings of the collected diffraction patterns yielded lattice parameters of comparable quality up to 34 GPa. These results suggest that antiferromagnetic $Bi_{2.1}Sr_{1.9}CaCu_2O_{8+\delta}$ retains an orthorhombic structure throughout the studied pressure range. Figure 4d illustrates the pressure dependence of lattice parameters along the *a*, *b*, and *c* axes. Figure 4e presents the corresponding unit-cell volume *V*, with $Z = 4$ representing the number of chemical formulas per unit cell. With increasing pressure, both the lattice parameters and the cell volume gradually decrease. The curve in Figure 4e shows the pressure−volume data fitted using the third-order Birch−Murnaghan equation of state (EOS).[53] The fitting results in a bulk modulus at a zero pressure (B_0) of 119.1 ± 4.7 GPa, an initial unit cell volume per chemical formula (V_0/Z) of 222.8 ± 0.2 Å^3, and a first pressure derivative of the bulk modulus at a zero pressure (B0′) of 9.8 ± 0.5 for antiferromagnetic $Bi_{2.1}Sr_{1.9}CaCu_2O_{8+\delta}$. The obtained B_0 value exceeds that reported for underdoped Bi-2212 (B_0 = 114.9 ± 6.4 GPa[52]) and is significantly higher than values reported for Bi-based cuprates (73,[54] 62.5,[51] and 68.6 GPa[55]). The significant variation in the B_0 values can be attributed to differences in sample composition and experimental conditions.

Among all discovered cuprate superconductors, bilayer Bi-2212 is the most extensively studied system, featuring a complete phase diagram[56,57] across the entire doping range from slightly underdoped to heavily overdoped regions. Interestingly, the structural properties of this system, in relation to the oxygen content across the entire doping range, remain underexplored. To date, a systematic analysis of the lattice parameter(s) evolution with doping for Bi-2212 across a wide doping range is lacking,[58,59] likely due to the complexity of structure determination.[60−63] Annealing as-grown samples under increasing partial oxygen pressure results in a higher oxygen content. Under these conditions, it was reported that T_c decreases with oxygen pressure, paralleling the reduction of the *c*-axis lattice constant.[58] This observation suggests that the *c*-axis lattice parameter decreases in the overdoped regime. Conversely, a similar decrease in the *c*-axis lattice parameter was observed with oxygen loss in single-phase Bi-2212.[59] Despite the exact *c* values not matching across different as-grown samples, both sets of experiments indicate a consistent decrease in the *c*-axis lattice parameter with carrier concentration.[58,59] No clear trends were observed for the lattice parameters along the *a* and *b* axes in these experiments.[58,59]

3.4. Relation between the In-Plane Superexchange Interaction *J* and the Lattice Parameter.

After establishing the pressure dependence of ω2 M and the EOS for antiferromagnetic $Bi_{2.1}Sr_{1.9}CaCu_2O_{8+\delta}$, we can derive the lattice parameter dependence of ω_{2M} by converting the pressure values to lattice parameters. This dependence, for the in-plane superexchange interaction *J*, can be directly calculated using formula $\omega_{2M} = 2.7J$.[44] In layered cuprates, the in-plane superexchange interaction, *J*, shows insensitivity to out-of-plane coupling. Thus, only the parameters within the CuO_2 plane are considered. A slight difference exists between the lattice parameters along the *a* and *b* axes in the antiferromagnetic $Bi_{2.1}Sr_{1.9}CaCu_2O_{8+\delta}$. Defining the average lattice constant in the *a*−*b* plane as $d = \sqrt{ab}$ is reasonable. The *d* value, corresponding to a given pressure for ω_{2M} (or *J*), is derived from the EOS, using the formula $V/Z = d^2\, c/4$.

To ascertain the exponent, *n*, for antiferromagnetic $Bi_{2.1}Sr_{1.9}CaCu_2O_{8+\delta}$, we plotted ln*J* as a function of ln*d* in Figure 5. Within 6 GPa, a linear relationship between ln*J* and ln*d* was observed. By conducting a linear fit of the ln*J*−ln*d* data within this pressure range, we derived the relationship $J \sim d^{-(6.6\pm0.2)}$. At pressures greater than 6 GPa, the relationship between ln *J* and ln*d* gradually deviates from linear with the deviation increasing as pressure rises. This suggests that the exponent, *n*, decreases with increasing pressure, indicating a reduced sensitivity of *J* to *d* at higher pressures, as was also observed in La_2CuO_4.[22] The observed behavior may be attributed to the sensitivity of the superexchange interaction to the angle in the Cu−O−Cu superexchange path,[64] especially if the buckling of the CuO_2 layers significantly increases above 10 GPa. The possible reasons for this behavior are discussed in the following section.

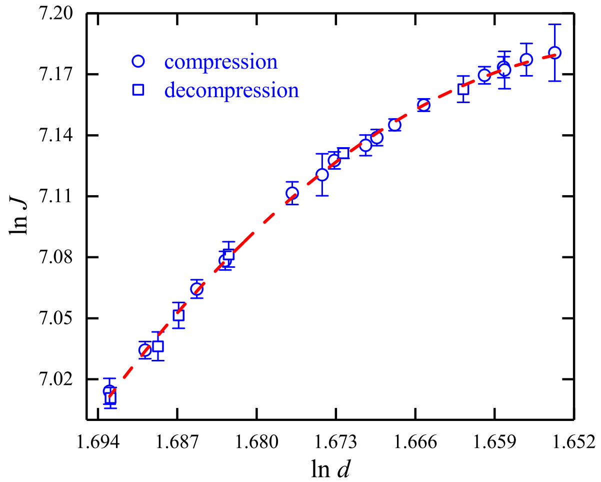

Figure 5. Double logarithmic plot of in-plane *J* versus the average in-plane lattice parameter, *d*. The dashed curve is the fitting to the data points.

Compared to other cuprates, the lattice parameter dependence of *J* in antiferromagnetic $Bi_{2.1}Sr_{1.9}CaCu_2O_{8+\delta}$ aligns closely with that of La_2CuO_4 ($J \sim d^{-(6.4\pm0.8)}$),[22] Eu_2CuO_4, and $YBa_2Cu_3O_{6.2}$ ($J \sim d^{-(3.0\pm0.5)}$),[25] as well as M_2CuO_4 (M = Pr, Nd, Sm, Eu, and Gd) ($J \sim d^{-(4\pm4.2)}$),[19] but significantly deviates from $Bi_{1.98}Sr_{2.06}Y_{0.68}CaCu_2O_{8+\delta}$ ($J \sim d^{-(10.33)}$).[26] Given that this relationship is established through simultaneous Raman and XRD measurements on the same characterized crystal under nearly identical experimental conditions, it is hoped to illuminate key aspects for the establishment and understanding of the superconductivity mechanism in high T_c cuprates.

3.5. Phonon Anomaly in the 10−15 GPa Range—A Possible Pressure-Induced Disorder?

Figure 6 illustrates the evolution of the phonon Raman spectra with increasing pressure. Panel (a) of Figure 6 provides a convenient overview of the spectra recorded, plotted as a function of wavenumber and pressure, using a false color. Above approximately 10 GPa, the low-frequency portion of the spectra develops a broad, featureless band. Within this band, the low-frequency A_{1g}

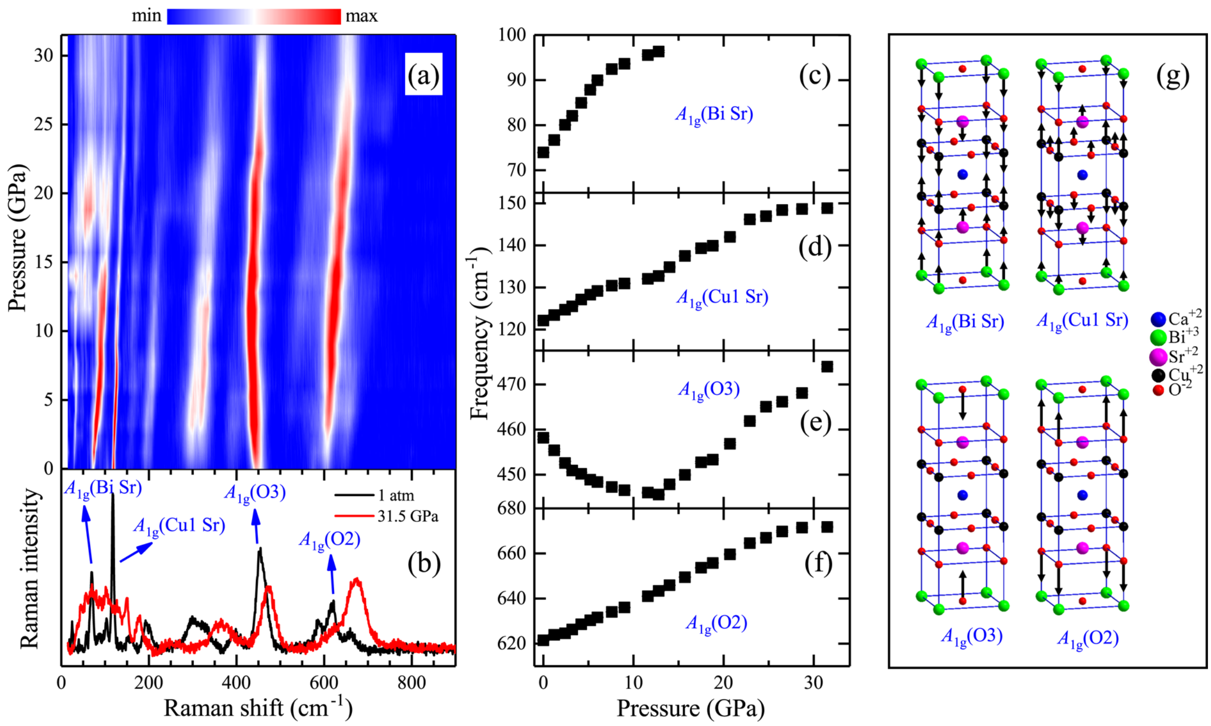

Figure 6. (a) Pressure dependence of the phonon frequencies in antiferromagnetic $Bi_{2.1}Sr_{1.9}CaCu_2O_{8+\delta}$ in the compression runs at various pressures. The phonon intensity is shown as a false color to visualize phonons in frequency−pressure variables in the 2d plane. (b) Comparison of the Raman spectra at 1 atm and at 31.5 GPa. The low-frequency range comparison shows clearly the disappearance of the Bi−Sr mode and broad “density of states”-like response. (c−f) Pressure dependence of selected phonon frequencies. Please note the softening of the O3 A_{1g} mode in the panel (e) up to 10−12 GPa, which corresponds to the oxygen vibration in the Bi−O charge reservoir layer.[46] (g) Schematic of the eigenvectors of the four lattice modes from panels (c−f).

mode—associated with the combined vibrations of Sr and Bi atoms—merges and becomes undetectable. Panel (b) of Figure 6 compares the Raman spectrum at 1 atm with that obtained at a high pressure of 31.5 GPa. The clearly visible broad band at low frequencies is tentatively attributed to pressure-induced disorder in layers containing heavy atoms. Remarkably, the A_{1g} mode, indicative of the combined vibrations of Cu and Sr atoms, remains detectable, even at the maximum pressure tested (31.5 GPa). Consequently, the observed disorder effects are primarily attributed to the layers containing Bi (charge reservoirs). Another significant observation is the softening of the O3 oxygen (Bi−O layer) A_{1g} vibrational mode up to approximately 10 GPa. This mode is associated with the oxygen ion in the ionic-like insulating layer, with its frequency determined by the effective charge and the ionic bonding strength. At high pressures, a decrease in interatomic distances is expected, leading to the mode's softening, which can be attributed to a reduction in effective charge. Therefore, our findings lend support to the charge transfer model up to at least 10 GPa in the insulating Bi-2212 sample. However, above 10 GPa, this mode resumes its typical behavior of increasing with pressure, indicating that any remaining charge transfer is significantly less pronounced than that at pressures below 10 GPa. The absence of clear signatures of disorder effects in our structural data suggests that any disorder is subtle, maintaining the orthorhombic symmetry of the unit cell.

Studies indicate that pressure-induced structural distortions in cuprates directly affect the superconducting properties of $Tl_2Ba_2CaCu_2O_{8+\delta}$,[36] which shares the crystal structure with Bi-2212. It was found that lattice distortion coincides with the pressure at which T_c reaches its maximum. We hypothesize that this may be due to the buckling of the CuO_2 planes caused by structural distortion. The buckling of the CuO_2 planes, a key structural parameter, significantly influences the electronic structure, affecting the Fermi surface and the density of states.[65,66] Buckling of the CuO_2 planes is believed to lower the T_c.[66−74] This phenomenon explains why Hg-based cuprates exhibit the highest T_c among similar materials due to minimal buckling distortion in their CuO_2 planes, offering insights for enhancing T_c in high-T_c cuprates. Cuprate superconductors typically contain numerous defects in both the CuO_2 planes and the outer layers. Experiments on cationic substitution in two single-layer systems, $Bi_{2.0}Sr_{1.6}Ln_{0.4}CuO_{6+\delta}$ and $La_{1.85}Nd_ySr_{0.15}CuO_4$, revealed that disorder in SrO planes significantly impacts T_c.[75] By carefully selecting synthesis conditions and atomic doping, it is possible to minimize these defects. In fact, careful control of synthesis conditions to reduce defects in the SrO planes of Bi-2212 elevated the T_c to a record 98 K.[76] As noted in the previous section, at high pressures (>6 GPa), the relationship between ln$J$ and ln$d$ deviates from linear behavior, with the deviation increasing with pressure. We speculate that the observed behavior may be due to the sensitivity of the superexchange interaction to the angle in the Cu−O−Cu path,[64] especially if disorder effects significantly enhance the “buckling” of the CuO_2 layers above 10 GPa.

Identifying the specific structural features linked to the apparent slowdown of effective superexchange J at pressures above approximately 10 GPa would be highly valuable. This information could potentially be obtained through neutron diffraction studies or single-crystal XRD measurements with

https://doi.org/10.1021/acs.jpcc.3c08244
J. Phys. Chem. C 2024, 128, 7223−7234

comprehensive Rietveld refinement. Conducting these experiments in cuprates at pressures up to 30 GPa would be extremely challenging, to the best of our knowledge. Finally, we believe to have found evidence of negligible charge-transfer effects on the behavior of J above 10 GPa, as indicated by the pressure dependence of the oxygen O3 (Bi−O layer) A_{1g} vibrational mode. We plan to investigate this mode across a broader range of doping levels to determine its relation to the observed trend of T_c decrease above 10−15 GPa in Bi-based cuprates.

3.6. Examination of Possible Superconductivity under Pressure. Superconductivity in strongly correlated systems is widely believed to be induced by doping or pressure. This has been evidenced by similar T_c phase diagrams observed with both tuning methods in strongly correlated superconductors, including heavy Fermions[77−79] and iron-based compounds.[80−82] In such superconductors, lattice parameters exhibit similar behaviors under both pressure and chemical substitution.[82] Examining whether superconductivity can be induced in Bi-2212, akin to other strongly correlated systems, is a logical step. Consequently, we conducted magnetic susceptibility measurements on antiferromagnetic $Bi_{2.1}Sr_{1.9}CaCu_2O_{8+\delta}$ crystals under the same pressure conditions used for Raman scattering and XRD measurements, within a similar pressure range. Results of these high-pressure measurements, up to 30.2 GPa, are listed in Figure 7. Pressure was applied and measured at approximately 120 K, below which it was maintained nearly constant. Magnetic susceptibility data were collected during the warming run for each pressure level. For comparison, the temperature dependence of the signal for nearly optimally doped $Bi_{2.1}Sr_{1.9}CaCu_2O_{8+\delta}$ at ambient pressure is shown in the inset of Figure 7. In both experiments, the crystals were cut to nearly the same size for measurements.

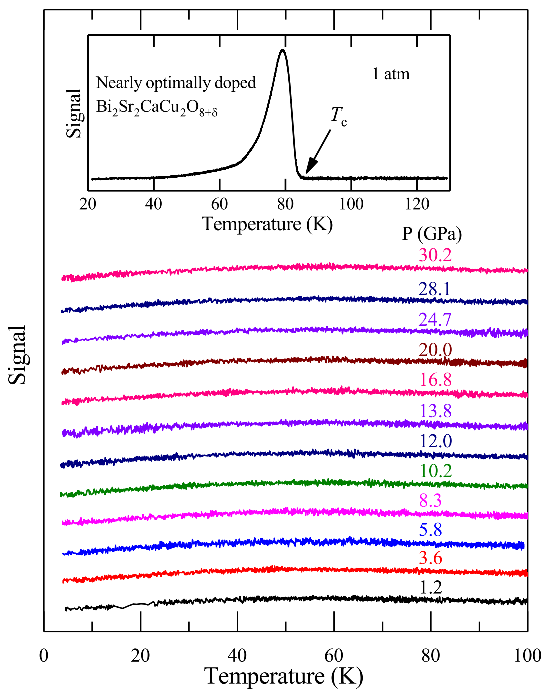

Figure 7. Magnetic susceptibility signal versus temperature for antiferromagnetic $Bi_{2.1}Sr_{1.9}CaCu_2O_{8+\delta}$ single crystal at applied pressures up to 30.2 GPa. Inset: magnetic susceptibility signal for nearly optimally doped $Bi_{2.1}Sr_{1.9}CaCu_2O_{8+\delta}$ at ambient pressure.

The magnetic susceptibility of nearly optimally doped $Bi_{2.1}Sr_{1.9}CaCu_2O_{8+\delta}$ shows a sharp rise to a peak against a flat baseline at 86 K and then decreases gradually with lower temperatures (see the inset of Figure 7). The initial rise from the high-temperature side signifies the superconducting transition, marked by the onset of the Meissner effect upon entering the superconducting state. This superconductivity characteristic has been documented in prior studies[30−33,35−37] using the established high-pressure magnetic measurement technique.[29]

Antiferromagnetic $Bi_{2.1}Sr_{1.9}CaCu_2O_{8+\delta}$ exhibited nearly identical and featureless signals across various pressures (Figure 7). This behavior markedly contrasts with the reference signal of nearly optimally doped $Bi_{2.1}Sr_{1.9}CaCu_2O_{8+\delta}$. Superconductivity characteristics were undetectable within the measured temperature and pressure ranges. Unlike heavy Fermions[77] or iron-based compounds,[81] antiferromagnetic $Bi_{2.1}Sr_{1.9}CaCu_2O_{8+\delta}$ does not exhibit superconductivity under pressures up to 30 GPa, as these observations show. Consequently, integrating this discovery with the phonon anomalies observed earlier, we conclude that the original charge-transfer model[35] does not apply to antiferromagnetic $Bi_{2.1}Sr_{1.9}CaCu_2O_{8+\delta}$ samples. This is consistent with recent discoveries of a pressure-induced transition to an insulating state in doped Bi-2212 superconductors.

3.7. What Parameters Matter for Superconductivity? The lack of superconductivity in the antiferromagnetic sample under pressure-induced lattice compression offers a unique opportunity to explore the critical parameters for superconductivity. Figure 4 shows that applying pressure significantly reduces the unit cell size of $Bi_{2.1}Sr_{1.9}CaCu_2O_{8+\delta}$. Above 10 GPa, the pressure-induced doping decreased significantly and failed to induce superconductivity. Conversely, pair formation is crucial for a system to become superconducting. In high-T_c cuprates, doping typically leads to a decrease in J.[9,11−15,48,49] Thus, if spin-mediated pairing is effective, quasiparticles could gain the energy needed for pairing at the expense of J.[17] The increase in J observed in $Bi_{2.1}Sr_{1.9}CaCu_2O_{8+\delta}$ under pressure (see Figure 3) suggests that antiferromagnetic order remains intact within the studied pressure range. If antiferromagnetism in this compound can be fully suppressed, then it may become possible to induce superconductivity.

The nearly constant pressure derivative of T_c (dT_c/dP)[56] and the universal parabolic evolution of T_c with pressure[35] in Bi-2212, regardless of oxygen content, suggest that factors other than carrier concentration from chemical doping or elemental substitution influence superconductivity. Given that the charge-transfer hypothesis is not corroborated by experimental data, it implies that factors other than doping must influence the T_c. The consistent magnetic excitations across the entire doping regime of the phase diagram in $La_{2-x}Sr_xCuO_4$[83] suggest that factors other than magnetic excitations may determine T_c. An inelastic neutron scattering study of $La_{2-x}Sr_xCuO_4$ showed a significant interaction between spin excitations and optical phonons.[84] This interaction could play a crucial role in forming charge density wave states and superconductivity in these materials.[85] Quantitative spectroscopic analysis of one-dimensional antiferromagnetic cuprate chains[86] indicates that the notably strong near-neighbor attraction likely stems from electron−

https://doi.org/10.1021/acs.jpcc.3c08244
J. Phys. Chem. C 2024, 128, 7223−7234

phonon coupling. The significant oxygen isotope effect and its evolution with the addition of CuO_2 planes in $Bi_2Sr_2Ca_{n-1}Cu_nO_{2n+4+\delta}$ (n = 1,2,3)[87] are difficult to explain without considering electron−phonon interactions. Time-resolved spectroscopy allows for distinguishing between electronic and phononic contributions to pairing strengths, thanks to their differing lifetimes.[88,89] Studies have shown that neither electronic excitations nor electron−phonon interactions can be overlooked.[88,89] In Bi-2212, the electron−phonon coupling strength mirrors T_c behavior in response to doping, whereas electron-spin fluctuation coupling strength consistently decreases with increased doping.[89] Thus, the pairing strength serves as a parameter independent of the carrier concentration. Inducing strong interactions through lattice compression and suppressing antiferromagnetic order may lead to superconductivity in $Bi_{2.1}Sr_{1.9}CaCu_2O_{8+\delta}$. The observed superconductivity in $Bi_{1.98}Sr_{2.06}Y_{0.68}CaCu_2O_{8+\delta}$[90] under modest pressure is likely attributed to enhanced interactions via lattice modulation from Y substitution. The phonon and two-magnon anomalies in $Bi_{1.98}Sr_{2.06}Y_{0.68}CaCu_2O_{8+\delta}$[90] differ significantly from those in $Bi_{2.1}Sr_{1.9}CaCu_2O_{8+\delta}$, suggesting distinct charge-transfer patterns that may explain the differences in ln$J$ versus ln$d$ dependencies.

As previously noted, Hg-based cuprates exhibit the highest T_c among similar layered materials, attributed to their CuO_2 planes having the least buckling distortion among cuprates. High-pressure application to a cuprate sample, already superconducting at ambient pressure, typically raises the critical temperature, T_c, at least in the initial stages. A significant previous finding is the increase of T_c from 134 to 164 K in Hg-1223,[91] marking the highest T_c recorded in cuprates. The 20−30% T_c increase in Hg-cuprates,[91] from ambient pressure to about 30 GPa, aligns well with the two-magnon excitation percentage increase shown in Figure 3. Viewing Hg cuprates as model systems for the T_c optimization potential, our results suggest a correlation between this potential and the Raman two-magnon energy, indicative of the superexchange interaction in cuprates. However, T_c (P) in Bi-based cuprates exhibits a more complex behavior, with a universal T_c decrease of around 10−15 GPa across various doping levels,[35] and a subsequent T_c increase at higher pressures in triple-,[30] single-, and double-layer Bi-based cuprates.[92] The discovery of an insulating phase in Bi-2212 at doping levels above 30−40 GPa[47] introduces controversy in higher pressure ranges, suggesting the system's sensitivity to stress conditions under different pressure media. Therefore, the link between J and superconductivity under pressure is a significant challenge in Bi-based superconductors. Our findings reveal that, even in antiferromagnetic compounds, two-magnon scattering up to 30 GPa does not follow the simple exponential function $J \sim d^{-n}$ seen in other antiferromagnetic compounds. These effects could be due to subtle structural changes, such as buckling, or pressure-induced doping. Our results indicate that antiferromagnetic Bi-2212 remains nonsuperconducting and possibly insulating up to 30 GPa. Consequently, we exclude doping effects from our $J(P)$ discussion in antiferromagnetic samples and hoped future transport property studies under pressure will provide clarity.

Considering that RIXS data indicate a nearly doping-independent superexchange parameter, J, our findings suggest that an increase in J under pressure could enhance superconductivity if J directly influences superconducting coupling, as proposed in various studies. However, structural effects such as buckling directly impact J, decreasing it when the superexchange path strays from the ideal 180° geometry. Our study offers crucial insights into the superexchange interaction J in a parent compound, yet key structural details are missing for a comprehensive understanding of Bi-based cuprates under pressure.

Pressure-induced doping complicates T_c behavior in doped compounds, potentially leading to nonmonotonic changes within a few tens of GPa, as recently demonstrated.[47] However, we believe that discussions on doped compounds should await reliable data on pressure-induced doping across the entire doping spectrum.

4. CONCLUSIONS

In conclusion, our comprehensive study of antiferromagnetic $Bi_{2.1}Sr_{1.9}CaCu_2O_{8+\delta}$ under high pressures employed Raman scattering, XRD, and magnetic susceptibility measurements. Raman scattering showed the two-magnon frequency rising from about 3000 cm^{-1} at ambient pressure to 3550 cm^{-1} at 33.1 GPa. Additionally, we noted phonon anomalies, suggesting disorder in heavy atom (Bi) layers and reduced charge transfer from Bi−O layers above 10 GPa. Lattice parameters decreased monotonically with pressure, showing no signs of a structural transition within the examined pressure range. Under compression, the in-plane superexchange interaction J increased with pressure, following with respect to the in-plane spacing at low pressures. We discussed these parameters' implications on superconductivity. We detected no pressure-induced superconductivity in the antiferromagnetic $Bi_{2.1}Sr_{1.9}CaCu_2O_{8+\delta}$ over the studied pressure range. Increasing evidence on superexchange's role in pairing suggests that reducing lattice constants and achieving optimal doping could significantly raise the sample's T_c over its ambient-pressure counterpart. However, Bi-based superconductors show multiple anomalous T_c (P) phenomena,[30,47,92] indicating the need for mechanisms beyond superexchange to fully understand them.

■ AUTHOR INFORMATION

Corresponding Author

Viktor V. Struzhkin − *Center for High Pressure Science and Technology Advanced Research, Shanghai 201203, China*; Email: viktor.struzhkin@hpstar.ac.cn

Authors

Jie Xin − *Department of Physics and State Key Laboratory of Surface Physics, Fudan University, Shanghai 200438, China; Center for High Pressure Science and Technology Advanced Research, Shanghai 201203, China*; orcid.org/0009-0000-2395-151X

Alexander G. Gavriliuk − *Institute for Nuclear Research, Russian Academy of Sciences, Moscow, Troitsk 108840, Russia; FSRC Crystallography and Photonics of Russian Academy of Sciences, Moscow 119333, Russia; REC Functional Nanomaterials, Immanuel Kant Baltic Federal University, Kaliningrad 236041, Russia*; orcid.org/0000-0003-0604-586X

Jia-Wei Hu − *Center for High Pressure Science and Technology Advanced Research, Shanghai 201203, China*

Jian-Bo Zhang − *Center for High Pressure Science and Technology Advanced Research, Shanghai 201203, China*; orcid.org/0000-0002-8339-1099

https://doi.org/10.1021/acs.jpcc.3c08244
J. Phys. Chem. C 2024, 128, 7223−7234

Gen-Da Gu − *Condensed Matter Physics and Materials Science, Brookhaven National Laboratory, Upton, New York 11973, United States*

Alexander F. Goncharov − *Earth and Planets Laboratory, Carnegie Institution for Science, Washington, District of Columbia 20015, United States;* orcid.org/0000-0002-6422-8819

Hai-Qing Lin − *School of Physics, Zhejiang University, Hangzhou 310058, China*

Ho-Kwang Mao − *Center for High Pressure Science and Technology Advanced Research, Shanghai 201203, China*

Xiao-Jia Chen − *Center for High Pressure Science and Technology Advanced Research, Shanghai 201203, China; School of Science, Harbin Institute of Technology, Shenzhen 518055, China;* orcid.org/0000-0003-3921-9424

Complete contact information is available at: https://pubs.acs.org/10.1021/acs.jpcc.3c08244

Notes

The authors declare no competing financial interest.

■ ACKNOWLEDGMENTS

The work at HPSTAR was supported by the National Key R&D Program of China (grant no. 2018YFA0305900). The work at HIT was supported from the Shenzhen Science and Technology Program (grant no. KQTD20200820113045081) and the Basic Research Program of Shenzhen (grant no. JCYJ20200109112810241). A.G.G. acknowledges to RSCF 21-12-00344 grant for help with high-pressure diamond anvils cell preparation. G.D.G was supported by the U.S. Department of Energy (DOE) (DE-SC0012704). V.V.S. and H.K.M. acknowledge the financial support from Shanghai Science and Technology Committee, China (no. 22JC1410300) and the Shanghai Key Laboratory of Materials Frontier Research in Extreme Environments, China (no. 22dz2260800). The XRD measurements were performed at HPCAT (Sector 16), APS, Argonne National Laboratory. HPCAT operations are supported by the DOE-NNSA's Office of Experimental Sciences. The APS is a U.S. DOE Office of Science User Facility operated for the DOE Office of Science by Argonne National Laboratory under contract no. DE-AC02-06CH11357.

■ REFERENCES

(1) Bednorz, J. G.; Müller, K. A. Possible high T_c superconductivity in the Ba-La-Cu-O system. *Z. Phys. B* **1986**, *64*, 189−193.

(2) Wu, M. K.; Ashburn, J. R.; Torng, C. J.; Hor, P. H.; Meng, R. L.; Gao, L.; Huang, Z. J.; Wang, Y. Q.; Chu, C. W. Superconductivity at 93 K in a new mixed-phase Y-Ba-Cu-O compound system at ambient pressure. *Phys. Rev. Lett.* **1987**, *58*, 908−910.

(3) Anderson, P. W. The resonating valence bond state in La_2CuO_4 and superconductivity. *Science* **1987**, *235*, 1196−1198.

(4) Anderson, P. W.; Lee, P. A.; Randeria, M.; Rice, T. M.; Trivedi, N.; Zhang, F. C. The physics behind high-temperature superconducting cuprates: The 'plain vanilla' version of RVB. *J. Phys.: Condens. Matter* **2004**, *16*, R755−R769.

(5) Monthoux, P.; Balatsky, A. V.; Pines, D. Weak-coupling theory of high-temperature superconductivity in the antiferromagnetically correlated copper oxides. *Phys. Rev. B: Condens. Matter Mater. Phys.* **1992**, *46*, 14803−14817.

(6) Scalapino, D. J. A common thread: The pairing interaction for unconventional superconductors. *Rev. Mod. Phys.* **2012**, *84*, 1383−1417.

(7) Devereaux, T. P.; Hackl, R. Inelastic light scattering from correlated electrons. *Rev. Mod. Phys.* **2007**, *79*, 175−233.

(8) Lyons, K. B.; Fleury, P. A.; Remeika, J. P.; Cooper, A. S.; Negran, T. J. Dynamics of spin fluctuations in lanthanum cuprate. *Phys. Rev. B: Condens. Matter Mater. Phys.* **1988**, *37*, 2353−2356.

(9) Sugai, S.; Shamoto, S. I.; Sato, M. Two-magnon Raman scattering in $(La_{1-x}Sr_x)_2CuO_4$. *Phys. Rev. B: Condens. Matter Mater. Phys.* **1988**, *38*, 6436−6439.

(10) Singh, R. R. P.; Fleury, P. A.; Lyons, K. B.; Sulewski, P. E. Quantitative Determination of Quantum Fluctuations in the Spin-1/2 Planar Antiferromagnet. *Phys. Rev. Lett.* **1989**, *62*, 2736−2739.

(11) Lyons, K. B.; Fleury, P. A.; Schneemeyer, L. F.; Waszczak, J. V. Spin fluctuations and superconductivity in $Ba_2YCu_3O_{6+\delta}$. *Phys. Rev. Lett.* **1988**, *60*, 732−735.

(12) Sugai, S.; Hosokawa, T. Relation between the superconducting gap energy and the two-magnon Raman peak energy in $Bi_2Sr_2Ca_{1-x}Y_xCu_2O_{8+\delta}$. *Phys. Rev. Lett.* **2000**, *85*, 1112−1115.

(13) Sugai, S.; Suzuki, H.; Takayanagi, Y.; Hosokawa, T.; Hayamizu, N. Carrier-density-dependent momentum shift of the coherent peak and the LO phonon mode in p-type high-T_c superconductors. *Phys. Rev. B: Condens. Matter Mater. Phys.* **2003**, *68*, 184504.

(14) Zaitsev, S. V.; Maksimov, A. A.; Tartakovskii, I. I. Two-magnon Raman scattering in dielectric and superconducting $YBa_2Cu_3O_{6+x}$ crystals. *J. Exp. Theor. Phys.* **2010**, *111*, 582−590.

(15) Li, Y.; Le Tacon, M.; Bakr, M.; Terrade, D.; Manske, D.; Hackl, R.; Ji, L.; Chan, M. K.; Barišić, N.; Zhao, X.; et al. Feedback effect on high-energy magnetic fluctuations in the model high-temperature superconductor $HgBa_2CuO_{4+\delta}$ observed by electronic Raman scattering. *Phys. Rev. Lett.* **2012**, *108*, 227003.

(16) Mansart, B.; Lorenzana, J.; Mann, A.; Odeh, A.; Scarongella, M.; Chergui, M.; Carbone, F. Coupling of a high-energy excitation to superconducting quasiparticles in a cuprate from coherent charge fluctuation spectroscopy. *Proc. Natl. Acad. Sci. U.S.A.* **2013**, *110*, 4539−4544.

(17) Lin, N.; Gull, E.; Millis, A. J. Two-particle response in cluster dynamical mean-field theory: Formalism and application to the Raman response of high-temperature superconductors. *Phys. Rev. Lett.* **2012**, *109*, 106401.

(18) Wang, L.; He, G. H.; Yang, Z. C.; Garcia-Fernandez, M.; Nag, A.; Zhou, K. J.; Minola, M.; Le Tacon, M.; Keimer, B.; Peng, Y. Y.; et al. Paramagnons and high-temperature superconductivity in a model family of cuprates. *Nat. Commun.* **2022**, *13*, 3163.

(19) Cooper, S. L.; Thomas, G. A.; Millis, A. J.; Sulewski, P. E.; Orenstein, J.; Rapkine, D. H.; Cheong, S. W.; Trevor, P. L. Optical studies of gap, exchange, and hopping energies in the insulating cuprates. *Phys. Rev. B: Condens. Matter Mater. Phys.* **1990**, *42*, 10785−10788.

(20) Mao, H. K.; Chen, X. J.; Ding, Y.; Li, B.; Wang, L. Solids, liquids, and gases under high pressure. *Rev. Mod. Phys.* **2018**, *90*, 015007.

(21) Goncharov, A. F.; Struzhkin, V. V. Raman spectroscopy of metals, high-temperature superconductors and related materials under high pressure. *J. Raman Spectrosc.* **2003**, *34*, 532−548.

(22) Aronson, M. C.; Dierker, S. B.; Dennis, B. S.; Cheong, S. W.; Fisk, Z. Pressure dependence of the superexchange interaction in antiferromagnetic La_2CuO_4. *Phys. Rev. B: Condens. Matter Mater. Phys.* **1991**, *44*, 4657−4660.

(23) Eremets, M. I.; Lomsadze, A. V.; Struzhkin, V. V.; Maksimov, A. A.; Puchkov, A. V.; Tartakovskii, I. I. Effect of high hydrostatic pressure on the exchange interaction in Eu_2CuO_4 single crystals. *Pis'maZh. Eksp. Teor. Fiz.* **1991**, *54*, 376.

(24) Struzhkin, V. V.; Goncharov, A. F.; Mao, H. K.; Hemley, R. J.; Moore, S. W.; Graybeal, J. M.; Sarrao, J.; Fisk, Z. Coupled magnon-phonon excitations in $Sr_2CuCu_2O_2$ at high pressure. *Phys. Rev. B: Condens. Matter Mater. Phys.* **2000**, *62*, 3895−3899.

(25) Maksimov, A.; Tartakovskii, I. Electronic and two-magnon light scattering in oxide superconducting crystals. *J. Supercond.* **1994**, *7*, 439−443.

(26) Cuk, T.; Struzhkin, V. V.; Devereaux, T. P.; Goncharov, A. F.; Kendziora, C. A.; Eisaki, H.; Mao, H. K.; Shen, Z. X. Uncovering a pressure-tuned electronic transition in $Bi_{1.98}Sr_{2.06}Y_{0.68}Cu_2O_{8+\delta}$ using Raman scattering and X-ray diffraction. *Phys. Rev. Lett.* **2008**, *100*, 217003.

(27) Kakihana, M.; Osada, M.; Käll, M.; Börjesson, L.; Mazaki, H.; Yasuoka, H.; Yashima, M.; Yoshimura, M. Raman-active phonons in $Bi_2Sr_2Ca_{1-x}Y_xCu_2O_{8+d}$ (x = 0−1): Effects of hole filling and internal pressure induced by Y doping for Ca, and implications for phonon assignments. *Phys. Rev. B: Condens. Matter Mater. Phys.* **1996**, *53*, 11796−11806.

(28) Gu, G. D.; Takamuku, K.; Koshizuka, N.; Tanaka, S. Large single crystal Bi-2212 along the c-axis prepared by floating zone method. *J. Cryst. Growth* **1993**, *130*, 325−329.

(29) Timofeev, Y. A.; Struzhkin, V. V.; Hemley, R. J.; Mao, H. K.; Gregoryanz, E. A. Improved techniques for measurement of superconductivity in diamond anvil cells by magnetic susceptibility. *Rev. Sci. Instrum.* **2002**, *73*, 371−377.

(30) Chen, X. J.; Struzhkin, V. V.; Yu, Y.; Goncharov, A. F.; Lin, C. T.; Mao, H. K.; Hemley, R. J. Enhancement of superconductivity by pressure-driven competition in electronic order. *Nature* **2010**, *466*, 950−953.

(31) Struzhkin, V. V.; Hemley, R. J.; Mao, H. K.; Timofeev, Y. A. Superconductivity at 10−17 K in compressed sulphur. *Nature* **1997**, *390*, 382−384.

(32) Struzhkin, V. V.; Eremets, M. I.; Gan, W.; Mao, H. K.; Hemley, R. J. Superconductivity in dense lithium. *Science* **2002**, *298*, 1213−1215.

(33) Chen, X. J.; Struzhkin, V. V.; Wu, Z. G.; Cohen, R. E.; Kung, S.; Mao, H. K.; Hemley, R. J.; Christensen, A. N. Electronic stiffness of a superconducting niobium nitride single crystal under pressure. *Phys. Rev. B: Condens. Matter Mater. Phys.* **2005**, *72*, 094514.

(34) Chen, X. J.; Struzhkin, V. V.; Wu, Z. G.; Lin, H. Q.; Hemley, R. J.; Mao, H. K. Unified picture of the oxygen isotope effect in cuprate superconductors. *Proc. Natl. Acad. Sci. U.S.A.* **2007**, *104*, 3732−3735.

(35) Chen, X. J.; Struzhkin, V. V.; Hemley, R. J.; Mao, H. K.; Kendziora, C. High-pressure phase diagram of $Bi_2Sr_2CaCu_2O_{8+\delta}$ single crystals. *Phys. Rev. B: Condens. Matter Mater. Phys.* **2004**, *70*, 214502.

(36) Zhang, J. B.; Struzhkin, V. V.; Yang, W. G.; Mao, H. K.; Lin, H. Q.; Ma, Y. C.; Wang, N. L.; Chen, X. J. Effects of pressure and distortion on superconductivity in $Tl_2Ba_2CaCu_2O_{8+\delta}$. *J. Phys.: Condens. Matter* **2015**, *27*, 445701.

(37) Wang, S. B.; Zhang, J. B.; Yan, J. Y.; Chen, X. J.; Struzhkin, V. V.; Tabis, W.; Barišić, N.; Chan, M. K.; Dorow, C.; Zhao, X. D.; et al. Strain derivatives of T_c in $HgBa_2CuO_{4+\delta}$: The CuO_2 plane alone is not enough. *Phys. Rev. B: Condens. Matter Mater. Phys.* **2014**, *89*, 024515.

(38) Mao, H. K.; Xu, J. A.; Bell, P. M. Calibration of the ruby pressure gauge to 800 kbar under quasi-hydrostatic conditions. *J. Geophys. Res.* **1986**, *91*, 4673−4676.

(39) Hammersley, A. P.; Svensson, S. O.; Hanfland, M.; Fitch, A. N.; Hausermann, D. Two-dimensional detector software: From real detector to idealised image or two-theta scan. *High Pres. Res.* **1996**, *14*, 235−248.

(40) Toby, B. H.; Von Dreele, R. B. GSAS-II: The genesis of a modern open-source all purpose crystallography software package. *J. Appl. Crystallogr.* **2013**, *46*, 544−549.

(41) Fukushima, N.; Niu, H.; Ando, K. Electrical and magnetic properties in $Bi_2Sr_2Ca_{1-x}Y_xCu_2O_{8+\delta}$. *Jpn. J. Appl. Phys.* **1988**, *27*, L1432.

(42) Belevtsev, B. I.; Dalakova, N. V.; Panfilov, A. S.; Beliayev, E. Y. Anomalies of conductivity behavior near the paramagnetic antiferromagnetic transition in single-crystals $La_2CuO_{4+\delta}$. *Physica B* **2010**, *405*, 1307−1311.

(43) Maeda, A.; Hase, M.; Tsukada, I.; Noda, K.; Takebayashi, S.; Uchinokura, K. Physical properties of $Bi_2Sr_2Ca_{n-1}Cu_nO_y$ (n = 1,2,3). *Phys. Rev. B: Condens. Matter Mater. Phys.* **1990**, *41*, 6418−6434.

(44) Weber, W. H.; Ford, G. W. Simple model for the linewidth of the two-magnon Raman feature observed in high-T_c superconductors. *Phys. Rev. B: Condens. Matter Mater. Phys.* **1989**, *40*, 6890−6895.

(45) Liu, H. L.; Blumberg, G.; Klein, M. V.; Guptasarma, P.; Hinks, D. G. c-axis electronic Raman scattering in $Bi_2Sr_2CaCu_2O_{8+\delta}$. *Phys. Rev. Lett.* **1999**, *82*, 3524−3527.

(46) Kovaleva, N. N.; Boris, A. V.; Holden, T.; Ulrich, C.; Liang, B.; Lin, C. T.; Keimer, B.; Bernhard, C.; Tallon, J. L.; Munzar, D.; et al. c-axis lattice dynamics in Bi-based cuprate superconductors. *Phys. Rev. B: Condens. Matter Mater. Phys.* **2004**, *69*, 054511.

(47) Zhou, Y.; Guo, J.; Cai, S.; Zhao, J.; Gu, G.; Lin, C.; Yan, H.; Huang, C.; Yang, C.; Long, S.; et al. Quantum phase transition from superconducting to insulating-like state in a pressurized cuprate superconductor. *Nat. Phys.* **2022**, *18*, 406−410.

(48) Blumberg, G.; Liu, R.; Klein, M. V.; Lee, W. C.; Ginsberg, D. M.; Gu, C.; Veal, B. W.; Dabrowski, B. Two-magnon Raman scattering in cuprate superconductors: Evolution of magnetic fluctuations with doping. *Phys. Rev. B: Condens. Matter Mater. Phys.* **1994**, *49*, 13295−13298.

(49) Rübhausen, M.; Rieck, C. T.; Dieckmann, N.; Subke, K. O.; Bock, A.; Merkt, U. Inelastic light scattering at high-energy excitations in doped cuprate superconductors. *Phys. Rev. B: Condens. Matter Mater. Phys.* **1997**, *56*, 14797−14808.

(50) Gao, Y.; Coppens, P.; Cox, D. E.; Moodenbaugh, A. R. Combined X-ray single-crystal and neutron powder refinement of modulated structures and application to the incommensurately modulated structure of $Bi_2Sr_2Ca_{1-x}Y_xCu_2O_{8+y}$. *Acta Crystallogr. A* **1993**, *49*, 141−148.

(51) Olsen, J. S.; Steenstrup, S.; Gerward, L.; Sundqvist, B. High pressure studies up to 50 GPa of Bi-based high-T_c superconductors. *Phys. Scr.* **1991**, *44*, 211−213.

(52) Zhang, J. B.; Tang, L. Y.; Zhang, J.; Qin, Z. X.; Zeng, X. J.; Liu, J.; Jin-Sheng, W.; Zhi-Jun, X.; Genda, G.; Chen, X. J. Pressure-induced isostructural phase transition in $Bi_2Sr_2CaCu_2O_{8+\delta}$. *Chin. Phys. C* **2013**, *37*, 088003.

(53) Birch, F. Finite elastic strain of cubic crystals. *Phys. Rev.* **1947**, *71*, 809−824.

(54) Tajima, Y.; Hikita, M.; Suzuki, M.; Hidaka, Y. Pressure-effect study on high-T_c superconducting single crystal of 84 K Bi-Sr-Ca-Cu-O system. *Physica C* **1989**, *158*, 237−240.

(55) Yu, J. D.; Sasaki, S.; Sugiura, H.; Huang, T.; Inaguma, Y.; Itoh, M. Compressibility and pressure dependence of charge transfer and T_c in pristine and iodine-intercalated single crystals of $Bi_{2.2}Sr_{1.8}CaCu_2O_{8+\delta}$. *Physica C* **1997**, *281*, 45−54.

(56) Sieburger, R.; Müller, P.; Schilling, J. S. Pressure dependence of the superconducting transition temperature in $Bi_2Sr_2CaCu_2O_{8+y}$ as a function of oxygen content. *Physica C* **1991**, *181*, 335−339.

(57) Drozdov, I. K.; Pletikosić, I.; Kim, C. K.; Fujita, K.; Gu, G. D.; Davis, J. C. S.; Johnson, P. D.; Božović, I.; Valla, T. Phase diagram of $Bi_2Sr_2CaCu_2O_{8+\delta}$ revisited. *Nat. Commun.* **2018**, *9*, 5210.

(58) Groen, W. A.; de Leeuw, D. Oxygen content, lattice constants and T_c of $Bi_2Sr_2CaCu_2O_{8+\delta}$. *Physica C* **1989**, *159*, 417−421.

(59) Liang, B.; Lin, C. T.; Maljuk, A.; Yan, Y. Effect of vacuum annealing on the structure and superconductivity of $Bi_2Sr_2CaCu_2O_{8+\delta}$ single crystals. *Physica C* **2002**, *366*, 254−262.

(60) Sunshine, S. A.; Siegrist, T.; Schneemeyer, L. F.; Murphy, D. W.; Cava, R. J.; Batlogg, B.; van Dover, R. B.; Fleming, R. M.; Glarum, S. H.; Nakahara, S.; et al. Structure and physical properties of single crystals of the 84-K superconductor $Bi_{2.2}Sr_2Ca_{0.8}Cu_2O_{8+\delta}$. *Phys. Rev. B: Condens. Matter Mater. Phys.* **1988**, *38*, 893−896.

(61) Gao, Y.; Lee, P.; Coppens, P.; Subramania, M. A.; Sleight, A. W. The incommensurate modulation of the 2212 Bi-Sr-Ca-Cu-O superconductor. *Science* **1988**, *241*, 954−956.

(62) Petricek, V.; Gao, Y.; Lee, P.; Coppens, P. X-ray analysis of the incommensurate modulation in the 2:2:1:2 Bi-Sr-Ca-Cu-O superconductor including the oxygen atoms. *Phys. Rev. B: Condens. Matter Mater. Phys.* **1990**, *42*, 387−392.

(63) Miles, P. A.; Kennedy, S. J.; McIntyre, G. J.; Gu, G. D.; Russell, G. S.; Koshizuka, N. Refinement of the incommensurate structure of

https://doi.org/10.1021/acs.jpcc.3c08244
J. Phys. Chem. C 2024, 128, 7223−7234

high quality Bi-2212 single crystals from a neutron diffraction study. *Physica C* **1998**, *294*, 275−288.
(64) Rocquefelte, X.; Schwarz, K.; Blaha, P. Theoretical investigation of the magnetic exchange interactions in copper (II) oxides under chemical and physical pressures. *Sci. Rep.* **2012**, *2*, 759.
(65) Chmaissem, O.; Jorgensen, J. D.; Short, S.; Knizhnik, A.; Eckstein, Y.; Shaked, H. Scaling of transition temperature and CuO_2 plane buckling in a high-temperature superconductor. *Nature* **1999**, *397*, 45−48.
(66) Schilling, J. S. High-pressure effects. *Handbook of High-Temperature Superconductivity*; Schrieffer, J. R., Brooks, J. S., Eds.; Springer: New York, 2007; pp 427−462.
(67) Dabrowski, B.; Wang, Z.; Rogacki, K.; Jorgensen, J. D.; Hitterman, R. L.; Wagner, J. L.; Hunter, B. A.; Radaelli, P. G.; Hinks, D. G. Dependence of superconducting transition temperature on doping and structural distortion of the CuO_2 planes in $La_{2-x}M_xCuO_4$ (M = Nd, Cr, Sr). *Phys. Rev. Lett.* **1996**, *76*, 1348−1351.
(68) Braden, M.; Hoffels, O.; Schnelle, W.; Büchner, B.; Heger, G.; Hennion, B.; Tanaka, I.; Kojima, H. Coupling between superconductivity and structural deformation in $La_{2-x}Sr_xCuO_4$ ($x \sim 0.13$). *Phys. Rev. B: Condens. Matter Mater. Phys.* **1993**, *47*, 12288−12291.
(69) Kaldis, E.; Röhler, J.; Liarokapis, E.; Poulakis, N.; Conder, K.; Loeffen, P. W. A displacive structural transformation in the CuO_2 planes of $YBa_2Cu_3O_x$ at the underdoped-overdoped phase separation line. *Phys. Rev. Lett.* **1997**, *79*, 4894−4897.
(70) Krüger, C.; Conder, K.; Schwer, H.; Kaldis, E. The dependence of the lattice parameters on oxygen content in orthorhombic $YBa_2Cu_3O_{6+x}$: A high precision reinvestigation of near equilibrium samples. *J. Solid State Chem.* **1997**, *134*, 356−361.
(71) Radaelli, P. G.; Wagner, J. L.; Hunter, B. A.; Beno, M. A.; Knapp, G. S.; Jorgensen, J. D.; Hinks, D. G. Structure, doping and superconductivity in $HgBa_2CaCu_2O_{6+\delta}$ ($T_c \leq 128$ K). *Physica C* **1993**, *216*, 29−35.
(72) Büchner, B.; Breuer, M.; Freimuth, A.; Kampf, A. P. Critical buckling for the disappearance of superconductivity in rare-earth-doped La2−xSrxCuO4. *Phys. Rev. Lett.* **1994**, *73*, 1841−1844.
(73) Yamada, N.; Ido, M. Pressure effects on superconductivity and structural phase transitions in $La_{2-x}M_xCuO_4$ (M = Ba, Sr). *Physica C* **1992**, *203*, 240−246.
(74) Takahashi, H.; Shaked, H.; Hunter, B. A.; Radaelli, P. G.; Hitterman, R. L.; Hinks, D. G.; Jorgensen, J. D. Structural effects of hydrostatic pressure in orthorhombic $La_{2-x}Sr_xCuO_4$. *Phys. Rev. B: Condens. Matter Mater. Phys.* **1994**, *50*, 3221−3229.
(75) Fujita, K.; Noda, T.; Kojima, K. M.; Eisaki, H.; Uchida, S. Effect of disorder outside the CuO_2 planes on T_c of copper oxide superconductors. *Phys. Rev. Lett.* **2005**, *95*, 097006.
(76) Hobou, H.; Ishida, S.; Fujita, K.; Ishikado, M.; Kojima, K. M.; Eisaki, H.; Uchida, S. Enhancement of the superconducting critical temperature in $Bi_2Sr_2CaCu_2O_{8+\delta}$ by controlling disorder outside CuO_2 planes. *Phys. Rev. B: Condens. Matter Mater. Phys.* **2009**, *79*, 064507.
(77) Mathur, N. D.; Grosche, F. M.; Julian, S. R.; Walker, I. R.; Freye, D. M.; Haselwimmer, R. K. W.; Lonzarich, G. G. Magnetically mediated superconductivity in heavy fermion compounds. *Nature* **1998**, *394*, 39−43.
(78) Park, T.; Ronning, F.; Yuan, H. Q.; Salamon, M. B.; Movshovich, R.; Sarrao, J. L.; Thompson, J. D. Hidden magnetism and quantum criticality in the heavy fermion superconductor $CeRhIn_5$. *Nature* **2006**, *440*, 65−68.
(79) Normile, P. S.; Heathman, S.; Idiri, M.; Boulet, P.; Rebizant, J.; Wastin, F.; Lander, G. H.; Le Bihan, T.; Lindbaum, A. High-pressure structural parameters of the superconductors $CeMIn_5$ and $PuMGa_5$ (M = Co,Rh). *Phys. Rev. B: Condens. Matter Mater. Phys.* **2005**, *72*, 184508.
(80) Rotter, M.; Tegel, M.; Johrendt, D. Superconductivity at 38 K in the iron arsenide $Ba_{1-x}K_xFe_2As_2$. *Phys. Rev. Lett.* **2008**, *101*, 107006.
(81) Alireza, P. L.; Ko, Y. T. C.; Gillett, J.; Petrone, C. M.; Cole, J. M.; Lonzarich, G. G.; Sebastian, S. E. Superconductivity up to 29 K in $SrFe_2As_2$ and $BaFe_2As_2$ at high pressures. *J. Phys.: Condens. Matter* **2008**, *21*, 012208.
(82) Kimber, S. A. J.; Kreyssig, A.; Zhang, Y. Z.; Jeschke, H. O.; Valenti, R.; Yokaichiya, F.; Colombier, E.; Yan, J. Q.; Hansen, T. C.; Chatterji, T.; et al. Similarities between structural distortions under pressure and chemical doping in superconducting $BaFe_2As_2$. *Nat. Mater.* **2009**, *8*, 471−475.
(83) Dean, M. P. M.; Dellea, G.; Springell, R. S.; Yakhou-Harris, F.; Kummer, K.; Brookes, N. B.; Liu, X.; Sun, Y. J.; Strle, J.; Schmitt, T.; et al. Persistence of magnetic excitations in $La_{2-x}Sr_xCuO_4$ from the undoped insulator to the heavily overdoped non-superconducting metal. *Nat. Mater.* **2013**, *12*, 1019−1023.
(84) Ikeuchi, K.; Wakimoto, S.; Fujita, M.; Fukuda, T.; Kajimoto, R.; Arai, M. Spin excitations coupled with lattice and charge dynamics in $La_{2-x}Sr_xCuO_4$. *Phys. Rev. B: Condens. Matter Mater. Phys.* **2022**, *105*, 014508.
(85) Struzhkin, V. V.; Chen, X. J. Magnon-phonon coupling and implications for charge-density wave states and superconductivity in cuprates. *Low Temp. Phys.* **2016**, *42*, 884−890.
(86) Chen, Z. Y.; Wang, Y.; Rebec, S. N.; Jia, T.; Hashimoto, M.; Lu, D. H.; Moritz, B.; Moore, R. G.; Devereaux, T. P.; Shen, Z. X. Anomalously strong near-neighbor attraction in doped 1D cuprate chains. *Science* **2021**, *373*, 1235−1239.
(87) Chen, X. J.; Liang, B.; Ulrich, C.; Lin, C. T.; Struzhkin, V. V.; Wu, Z. G.; Hemley, R. J.; Mao, H. K.; Lin, H. Q. Oxygen isotope effect in $Bi_2Sr_2Ca_{n-1}Cu_nO_{2n+4+\delta}$ (n = 1,2,3) single crystals. *Phys. Rev. B: Condens. Matter Mater. Phys.* **2007**, *76*, 140502.
(88) Dal Conte, S.; Giannetti, C.; Coslovich, G.; Cilento, F.; Bossini, D.; Abebaw, T.; Banfi, F.; Ferrini, G.; Eisaki, H.; Greven, M.; et al. Disentangling the electronic and phononic glue in a high-T_c superconductor. *Science* **2012**, *335*, 1600−1603.
(89) Chia, E. E. M.; Springer, D.; Nair, S. K.; Zou, X. Q.; Cheong, S. A.; Panagopoulos, C.; Tamegai, T.; Eisaki, H.; Ishida, S.; Uchida, S.; et al. Doping dependence of the electron-phonon and electron-spin fluctuation interactions in the high-T_c superconductor $Bi_2Sr_2CaCu_2O_{8+\delta}$. *New J. Phys.* **2013**, *15*, 103027.
(90) Cuk, T.; Zocco, D. A.; Eisaki, H.; Struzhkin, V.; Grosche, F. M.; Maple, M. B.; Shen, Z. X. Signatures of pressure-induced superconductivity in insulating $Bi_{1.98}Sr_{2.06}Y_{0.68}CaCu_2O_{8+\delta}$. *Phys. Rev. B: Condens. Matter Mater. Phys.* **2010**, *81*, 184509.
(91) Gao, L.; Xue, Y. Y.; Chen, F.; Xiong, Q.; Meng, R. L.; Ramirez, D.; Chu, C. W.; Eggert, J. H.; Mao, H. K. Superconductivity up to 164 K in $HgBa_2Ca_{m-1}Cu_mO_{2m+2+\delta}$ (m = 1, 2, and 3) under quasihydrostatic pressures. *Phys. Rev. B: Condens. Matter Mater. Phys.* **1994**, *50*, 4260−4263.
(92) Deng, L.; Zheng, Y.; Wu, Z.; Huyan, S.; Wu, H. C.; Nie, Y.; Cho, K.; Chu, C. W. Higher superconducting transition temperature bybreaking the universal pressure relation. *Proc. Natl. Acad. Sci. U.S.A.* **2019**, *116*, 2004−2008.

https://doi.org/10.1021/acs.jpcc.3c08244
J. Phys. Chem. C 2024, 128, 7223−7234